Operation and Control of 850kW Doubly Fed Induction Generators Based Al-Zafarana Egyptian Wind Farm

Khaled Hamza El-Sayed
Electrical Power and Machines Dept., Faculty of Engineering, Cairo University, Egypt
EE at Saudi Binladin Group (SBG), Cairo, Egypt
Email: eng.k.hamza@gmail.com

Doaa Khalil Ibrahim and Essam El-Din Abo El-Zahab
Electrical Power and Machines Dept., Faculty of Engineering, Cairo University, Egypt

***Abstract*—With increasing global great concern over greenhouse gas emissions and their harmful effects on environment, huge number of wind turbines are recently connected to electrical grids. Nowadays, Egypt has continuous development of wind energy projects; it makes a great effort at Gulf of Suez area especially in Al-Zafarana district. This paper focuses on studying the dynamic performance of the 5th phase of Al-Zafarana wind farm, which is made of 100 Gamesa G52/850kW Doubly Fed Induction Generator (DFIG) machines, using Digsilent/PowerFactory simulation tool as an advanced simulation package. As DFIG is currently one of the most common types employed for Wind Energy Conversion System (WECS), the paper also implements a dynamic model for 850kW DFIG machine based WECS in Matlab/Simulink environment. A dual reference frame control strategy is applied here to improve the dynamic system performance during balanced and unbalanced grid voltage conditions.**

***Index Terms*—Doubly Fed Induction Generator (DFIG), power generation control, unbalance grid voltage conditions, vector control, Wind Energy Conversion System (WECS)**

I. Introduction

Fossil fuels are still the back bone of energy production in many regions of the world; however their harmful environmental impacts on all living creatures have hit the danger horn to depend on new clean renewable energy resources.

Wind Energy Conversion System (WECS) has the leading position among other renewable energy resources due to its competitive cost of generated electrical power. Wind turbines can be classified into two types; fixed-speed and variable-speed turbines. The fixed-speed wind turbine is equipped with an induction generator which is directly connected to the grid and rotates at a constant speed regardless the wind speed. It is a simple and rugged system, but it has several drawbacks; one of them is the incapability of the system to absorb high fluctuations in torque and power at variable wind speed that cause terminal voltage variations which deteriorate system grid voltage [1], [2]. On the contrary, variable-speed wind turbine can operate smoothly at wind speed variations without any exported torque and power fluctuations due to its continuous adjusting of the wind turbine rotational speed with the wind speed. Therefore it reduces mechanical stresses and improves the power quality and hence the overall system efficiency.

Nowadays, variable-speed wind turbines equipped with Doubly Fed Induction Generator (DFIG) directly connected to the grid are widely used due to several features. DFIG can supply electrical power to the grid at constant voltage and constant frequency, while the rotor can operate at sub-synchronous mode or super-synchronous mode. Besides, DFIG's generated active and reactive power can be controlled independently, and the power converter is much cheaper as its rating is only about 30% of the total system power [3], [4].

With the high penetration of renewable resources in the electrical grids especially wind power, WECS are expected to behave as conventional power plants by accomplishing grid code requirements along with its operation status. Fault Ride Through (FRT) is considered one of the most extreme grid code requirements. This enables the wind turbine to continue in operation during different unbalanced grid voltage conditions and also to support terminal voltage by feeding reactive current to the grid [5]-[7]. As a result of the direct connection between the DFIG stator and the system grid, the unbalanced grid voltages induce unbalanced currents which cause significant oscillation ripples in torque, power and DC link voltages. The resultant torque ripples could lead into severe mechanical stresses on the drive train and gearbox as well as become a source of acoustic noise. The unbalanced currents also cause hot spot regions at stator and rotor windings that would decrease insulation's life time or cause complete insulation failure [8]. Hence, protective measures should be taken into consideration to achieve stable continuous operation

Manuscript received December 31, 2015; revised June 29, 2016.

©2016 International Journal of Electrical Energy

doi: 10.18178/ijoee.4.2.112-121

within grid code margins without further stresses on power converters.

In this paper, the 5th phase of Al-Zafarana wind farm is implemented using Digsilent/Powerfactory tool to study and analyze the dynamic operation of that wind farm during different grid voltage conditions to study and assess the influence of unbalanced grid voltage conditions on wind turbines. Gamesa G52/850kW DFIG machine, which is employed in Al-Zafarana (Phase-5), is also modeled and implemented with a dual sequence reference frame control scheme in Matlab/Simulink to improve its control system stability during balanced and unbalanced grid voltage conditions.

II. DFIG-Based Wind Energy Conversion Systems

Due to its vital advantages among other variable wind turbine types such as reduced converter sizing, reduced cost, and improved efficiency, DFIG dominates the wind energy market. Configuration of the overall DFIG-based WECS is depicted in Fig. 1. The stator winding is directly connected to the grid via a step up transformer, while the rotor winding is connected to the grid via two bi directional back to back Voltage Source Converters (VSC) linked by a DC bus and coupled with slip rings to rotor windings. Two levels VSC are commonly used, each consisting of six insulated bipolar transistors and respective antiparallel diodes. The Rotor Side Converter (RSC) is used to independently control the stator active and reactive output power from the machine by controlling independently the rotor current of the DFIG. RSC determines the rotor speed and the reference power, and then it regulates the active and reactive power by acting on rotor current components. The Grid Side Converter (GSC) is used to independently control the DC link voltage and to govern the active and reactive power exchange between rotor and system grid [4].

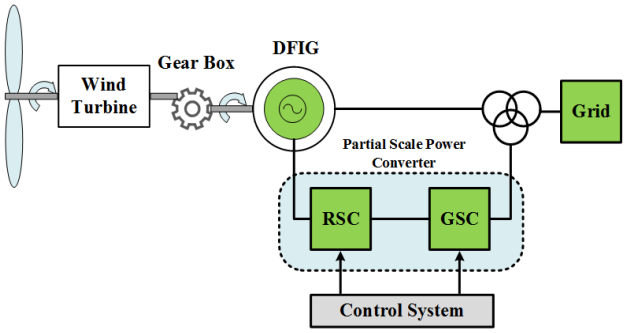

Figure 1. DFIG based WECS overall configuration scheme

The power converter scheme configuration is mainly used to decouple the electrical grid frequency from the mechanical rotor frequency, and to provide rotor voltage whose magnitude and phase angle are adjustable. This variable rotor voltage let the system makes continuous adjustment for the rotor speed at different wind speed variations. Hence rotor variable speed operation is normally enabled around ±30% of the synchronous speed. The power converter also enables the DFIG to work under the four quadrants in the complex PQ-plane, this means that the DFIG is capable to deliver and control reactive power exchange with the system grid [9], [10].

III. Modeling & Control of DFIG-Based WECS

DFIG modeling and control have been studied in details in [11]-[19]. Wind turbine model and DFIG model will be reviewed in the following sections.

A. Wind Turbine Modeling Equations

Wind turbine captures the mechanical energy from moving air streams by its rotating blades and converts them into electrical energy. As the kinetic energy stored in the moving air stream is function of the cube of wind speed, the wind power can be presented by [9], [11]:

$$P_w = \frac{1}{2}\,\rho\, A\, v_w^3 \tag{1}$$

where, P_w is the wind power (watt), ρ is the air density (kg/m^3), A is the rotor swept area (m^2), and v_w is moving stream wind speed (m/s).

Betz reveals the limit theory which states that the wind turbine can only convert less than 59.3% of the kinetic energy in moving air stream into mechanical energy. Therefore the mechanical power extracted from the wind is given by [12]:

$$P_m = C_p(\lambda,\beta)\,.P_w = \frac{1}{2}\,\rho\,.C_p(\lambda,\beta)\,.A\,.v_w^3 \tag{2}$$

where C_p is the dimensionless performance coefficient as a function of tip speed ratio $\lambda(\lambda = \frac{\omega_m\, R}{v_w})$, and blades pitch angle β as shown in Fig. 2. While ω_m is the rotor angular velocity (radians/sec) and the swept area $A = \pi R^2$ (R is the rotor blade radius in m). The performance coefficient C_p could be described by [14]:

$$C_p(\lambda,\beta) = 0.5\left[\frac{116}{\lambda_i} - 0.4\beta - 5\right].e^{\frac{-21}{\lambda_i}} \tag{3}$$

where,

$$\lambda_i = [(\lambda + 0.08\beta)^{-1} - 0.035/(\beta^3+1)]^{-1} \tag{4}$$

Therefore, the mechanical torque imposed on the turbine's rotor can be expressed from the mechanical power as follows:

$$T_m = \frac{P_m}{\omega_m} \tag{5}$$

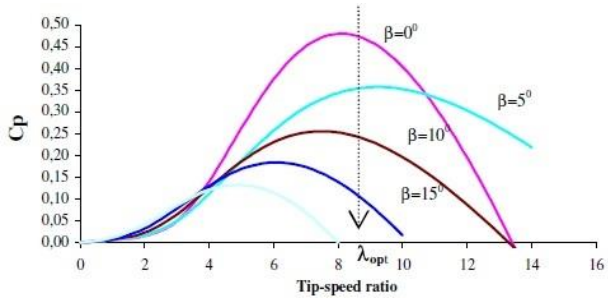

Figure 2. Power coefficient characteristic curve

B. DFIG Modeling Equations

DFIG has two main operation mode scenarios depending on the rotor speed [2], [18], as depicted in Fig. 3:

1. Sub-Synchronous mode, which is applicable when the rotor speed is lower than the synchronous speed. Thus, the slip is a positive fraction. Therefore the rotor receives power from the grid, while both the mechanical power and rotor power are then exported to the grid via stator windings.
2. Super-Synchronous mode, which is applicable when the rotor speed is higher than the synchronous speed. Thus, the slip is a negative fraction. Therefore the rotor exports power to the grid, and the mechanical power from wind is transferred to the grid via both stator and rotor windings.

DFIG is a complicated nonlinear system, therefore Park Model is usually utilized to simplify and analyze its behavior as explained in Fig. 4. Transformation into dq reference frame is one of the powerful tools in control scheme implementation to get all the time varying variables in DC values [17], [18]. DFIG equivalent circuit under synchronous dq reference frame is described in Fig. 5, and formulated by the Equations (6)-(15).

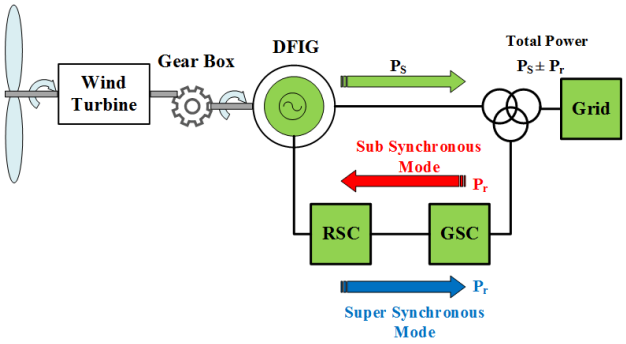

Figure 3. DFIG sub-synchronous & super-synchronous power flow modes

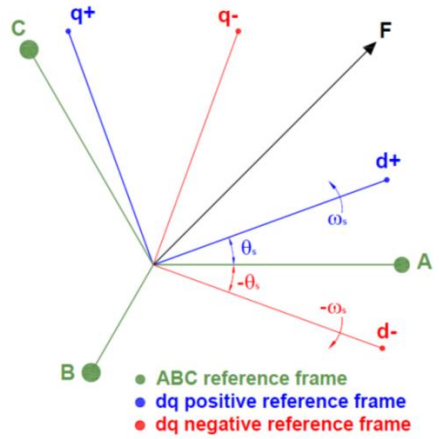

Figure 4. Spatial diagram of reference frames relationships

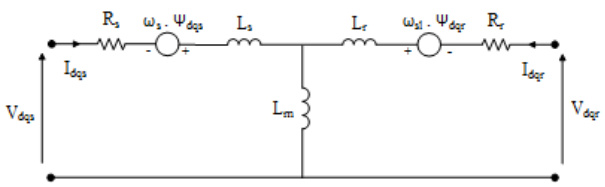

Figure 5. DFIG equivalent circuit in dq reference frame

Voltage Equations:

$$V_{ds} = I_{ds} R_s + \frac{d}{dt}\psi_{ds} - \omega_s \psi_{qs} \quad (6)$$

$$V_{qs} = I_{qs} R_s + \frac{d}{dt}\psi_{qs} + \omega_s \psi_{ds} \quad (7)$$

$$V_{dr} = I_{dr} R_r + \frac{d}{dt}\psi_{dr} - (\omega_s - \omega_r)\psi_{qr} \quad (8)$$

$$V_{qr} = I_{qr} R_r + \frac{d}{dt}\psi_{qr} + (\omega_s - \omega_r)\psi_{dr} \quad (9)$$

Flux Equations:

$$\psi_{ds} = L_s I_{ds} + L_m I_{dr} \quad (10)$$

$$\psi_{qs} = L_s I_{qs} + L_m I_{qr} \quad (11)$$

$$\psi_{dr} = L_m I_{ds} + L_r I_{dr} \quad (12)$$

$$\psi_{qr} = L_m I_{qs} + L_r I_{qr} \quad (13)$$

Electromagnetic Torque Equations:

$$T_{em} = n_p L_m \left(I_{qs} I_{dr} - I_{ds} I_{qr}\right) \quad (14)$$

$$T_{em} - T_m = \frac{J}{n_p} \times \frac{d}{dt}\omega_r \quad (15)$$

where: $V_{ds}, V_{qs}, V_{dr}, V_{qr}$ are the dq components of stator & rotor voltages respectively. I_{ds}, I_{qs}, I_{dr}, I_{qr} and ψ_{ds}, ψ_{qs}, ψ_{dr}, ψ_{qr} are the dq components of stator & rotor currents and their corresponding flux components respectively. R_s , R_r and ω_s, ω_r are the stator & rotor resistance and synchronous speed respectively. L_m is the magnetizing inductance. L_s , L_r are the stator & rotor self-inductance. T_{em} is the electromagnetic torque. T_m is the mechanical torque. J is the moment of inertia.

C. DFIG Control Principals

The main control objectives of DFIG-based WECS could be summarized in:

1. Maximizing the captured power from wind streams when wind speed is lower than rated values by adopting Maximum Point Tracking Technique (MPPT) strategy.
2. Limiting and controlling the output power and rotor speed when wind speed exceeds rated values by applying pitch angle control.
3. Controlling the DFIG to provide electrical power within system power quality standards.
4. Putting the DFIG system in the parking mode at higher wind gusts as a kind of protection.

Based on the Vector Oriented Control (VOC) Technique, RSC will be designed in Stator Flux Oriented Control (SFOC) by aligning the direct axis of the synchronous reference frame along with the stator flux vector, while the quadrature axis will be perpendicular to it.

$$\psi_{ds} = \psi_s \,, \; \psi_{qs} = 0 \quad (16)$$

By neglecting stator resistance, then stator voltage components could be given by:

$$V_{ds} = 0, \; V_{qs} = V_s \quad (17)$$

By applying these conditions on DFIG model equations, the stator active & reactive power formulae could be deduced by the following equations:

$$\begin{cases} P_s = V_{ds}.I_{ds} + V_{qs}.I_{qs} = -V_s \frac{L_m}{L_s} I_{qr} \\ Q_s = V_{qs}.I_{ds} - V_{ds}.I_{qs} = V_s \frac{\psi_s - L_m I_{dr}}{L_s} \end{cases} \quad (18)$$

As shown, the stator active & reactive power are decoupled and controlled independently by acting on the rotor current components. The direct component of rotor current I_{dr} is controlled to act on the stator reactive power, while the quadrature component of rotor current I_{qr} is controlled to act on the stator active power.

IV. DFIG Operation & Control under Unbalanced Grid Voltage Conditions

Unbalanced stator voltage conditions create negative sequence currents that cause high temperature rise, saturate the rotor side converter, and cause double oscillations in torque and power. To describe unbalanced three phase voltage system, the index of Voltage Unbalance Factor (VUF %), which is the percentage ratio of negative sequence voltage to positive sequence voltage components, is used [3], [5]. The behavior of DFIG under unbalanced grid voltage conditions is described in [20]-[23].

The rotor flux could be rewritten in terms of stator flux and rotor currents as:

$$\psi_r = \frac{L_m}{L_s} \psi_s + \sigma L_r I_r \quad (19)$$

where σ is the leakage factor ($\sigma = 1 - \frac{{L_m}^2}{L_s L_r}$).

By substituting in rotor voltage equation, the rotor voltage could be rewritten again by:

$$V_r = \frac{L_m}{L_s} \left(\frac{d}{dt} - j\omega_{sl}\right) \psi_s + \left(R_r + \sigma L_r \left(\frac{d}{dt} - j\omega_{sl}\right)\right) I_r \quad (20)$$

where ω_{sl} is the slip speed. It is clear that Eq. (20) is composed of two parts; the first part presents the electromagnetic force due to the stator flux induced in rotor winding, while the second part presents the voltage drop in both rotor resistance and reactance, which is a comparable small value. Thus, we can consider the rotor voltage to be equal to the induced emf. [20].

$$(e_r = \frac{L_m}{L_s} \left(\frac{d}{dt} - j\omega_{sl}\right).\psi_s)$$

Accordingly, we can conclude that the rotor induced emf mainly depends on both the slip and stator flux variation. Therefore any change in grid voltage as voltage unbalance will impact on the stator flux and consequently to the rotor induced emf.

A. DFIG Operation under Unbalanced Voltage Conditions

According to the symmetrical components theory, unbalanced three phase voltage in any power system could be resolved into three balanced sets; positive, negative, and zero sequence components [21]. By ignoring the zero sequence component, the stator voltage expression will be:

$$V_s = V_s^+ + V_s^- = V^+ e^{j\omega_s t} + V^- e^{-j\omega_s t} \quad (21)$$

The induced stator flux in steady state will be composed of two terms;

1. Forced flux, which is a rotational flux term. It is the summation of two components corresponding to the positive & negative sequence components of stator voltage.
2. Natural flux, which is a transient term appears because of the stator voltage change to guarantee that there is no discontinuity in stator flux.

Therefore the stator flux is composed of two steady state terms and one transient term as follows [21]:

$$\psi_s = \psi_s^+ + \psi_s^- + \psi_s^n = \frac{V^+}{J\omega_s} e^{j\omega_s t} + \frac{V^-}{-J\omega_s} e^{-j\omega_s t} + \psi_s^n e^{-t/\tau_s} \quad (22)$$

Each flux component will induce rotor voltage in the rotor windings depending on stator voltage amplitude and its relative speed, therefore the total emf at rotor terminal can be given by:

$$\mathrm{e_r} = \mathrm{e_r^+} + \mathrm{e_r^-} + \mathrm{e_r^n} = \frac{\mathrm{L_m}}{\mathrm{L_s}} \mathrm{V^+} \times s \times \mathrm{e}^{\mathrm{j}\omega_s t} + \frac{\mathrm{L_m}}{\mathrm{L_s}} \mathrm{V^-} \times (s-2) \times \mathrm{e}^{-\mathrm{j}\omega_s t} + \frac{\mathrm{L_m}}{\mathrm{L_s}} \left(\frac{1}{\tau_s} + \mathrm{j}\omega_r\right) \times \psi_s^n \times \mathrm{e}^{-t/\tau_s} \quad (23)$$

Emf formulae can be expressed in rotor reference frame as:

$$e_r{}^r = \frac{L_m}{L_s} V^+ \times s \times e^{js\omega_s t} + \frac{L_m}{L_s} V^- \times (s-2) \times e^{-j(s-2)\omega_s t} + \frac{L_m}{L_s} \left(\frac{1}{\tau_s} + j\omega_r\right) \times \psi_s^n \times e^{\left(\frac{1}{\tau_s} + j\omega_r\right)t} \quad (24)$$

It can be noted that the positive sequence rotor voltage will be proportional to the slip; hence it is a small value and exists in normal operation. But the negative sequence rotor voltage only exists in case of unbalanced conditions, and has a factor of two; hence it is very important component and will negatively affect the operation of the DFIG under asymmetrical voltage dips. The natural flux also will induce a transitory voltage which appears firstly in the dip and decays exponentially depending on its initial value; so this term appears at start and end of the dip occurrence [23].

If the total induced emf rotor voltage is greater than rotor side converter's rated voltage, it will cause machine loss of control.

B. DFIG Control under Unbalanced Voltage Conditions

DFIG control under unbalanced grid voltage conditions is well explained in many literatures as in [24]-[28]. In balanced grid voltage conditions, the impacts of negative sequence components are ignored when designing DFIG control scheme as it contains only control loops for positive sequence components. Therefore when unbalanced grid voltage condition exists, the conventional control scheme will not be able to

control or reduce the impacts of unbalanced grid conditions on DFIG due to the singularity process control of positive sequence components.

Hence an improved control scheme that handles the effects of negative sequence components is a must to enhance DFIG operation and to operate safely under both balanced and unbalanced grid voltage conditions. Dual sequence reference frame control strategy will be developed and applied to take control of both the positive and negative sequence components in synchronous reference frame at single control scheme structure. The main theme of dual control scheme is to measure the network currents, to separate both rotor positive and negative sequence components by using notch filter or low pass filter, and finally to control the rotor currents to be traced with the predefined reference values [25]. The rotor positive sequence current set, as in the conventional control scheme, is based on the controlling duties of stator active power (or electromagnetic torque) and stator reactive power. The rotor negative sequence current set is based on the corresponding unbalanced control targets, as listed in Table I.

TABLE I. DFIG CONTROL TARGETS DURING UNBALANCED CONDITIONS

Control Target	I_{dr-}^{-*}	I_{qr-}^{-*}
Balancing stator currents	ψ_{ds-}^{-} / L_m	ψ_{qs-}^{-} / L_m
Eliminating stator active power pulsations	$\frac{2\,\psi_{ds-}^{-}}{L_m} - \frac{\psi_{ds-}^{-}}{\psi_{ds+}^{+}}.I_{dr+}^{+} - \frac{\psi_{qs-}^{-}}{\psi_{ds+}^{+}}.I_{qr+}^{+}$	$\frac{2\,\psi_{qs-}^{-}}{L_m} - \frac{\psi_{qs-}^{-}}{\psi_{ds+}^{+}}.I_{dr+}^{+} + \frac{\psi_{ds-}^{-}}{\psi_{ds+}^{+}}.I_{qr+}^{+}$
Eliminating electromagnetic torque pulsations	$\frac{\psi_{ds-}^{-}}{\psi_{ds+}^{+}}.I_{dr+}^{+} + \frac{\psi_{qs-}^{-}}{\psi_{ds+}^{+}}.I_{qr+}^{+}$	$\frac{\psi_{qs-}^{-}}{\psi_{ds+}^{+}}.I_{dr+}^{+} - \frac{\psi_{ds-}^{-}}{\psi_{ds+}^{+}}.I_{qr+}^{+}$

The relationship between positive and negative sequence components in synchronous reference frame is described in the spatial diagram shown in Fig. 4. Therefore any machine variable (F) including voltage, current, and flux components will be shown in positive and negative sequence reference frames as follows:

$$\begin{cases} F_{dq}^{+} = F_{dq+}^{+} + F_{dq-}^{+} = F_{dq+}^{+} + F_{dq-}^{-}\mathrm{e}^{-\mathrm{j}2\omega_s t} \\ F_{dq}^{-} = F_{dq-}^{-} + F_{dq+}^{-} = F_{dq-}^{-} + F_{dq+}^{+}\mathrm{e}^{\mathrm{j}2\omega_s t} \end{cases} \quad (25)$$

Therefore the dynamic equations of DFIG with positive sequence components can be described by the following equations sets [26]:

$$\begin{pmatrix} V_{ds+}^{+} \\ V_{qs+}^{+} \end{pmatrix} = R_s \begin{pmatrix} I_{ds+}^{+} \\ I_{qs+}^{+} \end{pmatrix} + \frac{d}{dt}\begin{pmatrix} \psi_{ds+}^{+} \\ \psi_{qs+}^{+} \end{pmatrix} + j\omega_s^{+}\begin{pmatrix} 0 & -1 \\ 1 & 0 \end{pmatrix}\begin{pmatrix} \psi_{ds+}^{+} \\ \psi_{qs+}^{+} \end{pmatrix}$$

$$\begin{pmatrix} V_{dr+}^{+} \\ V_{qr+}^{+} \end{pmatrix} = R_r \begin{pmatrix} I_{dr+}^{+} \\ I_{qr+}^{+} \end{pmatrix} + \frac{d}{dt}\begin{pmatrix} \psi_{dr+}^{+} \\ \psi_{qr+}^{+} \end{pmatrix} + j\omega_{sl}^{+}\begin{pmatrix} 0 & -1 \\ 1 & 0 \end{pmatrix}\begin{pmatrix} \psi_{dr+}^{+} \\ \psi_{qr+}^{+} \end{pmatrix}$$

$$\begin{pmatrix} \psi_{dqs+}^{+} \\ \psi_{dqr+}^{+} \end{pmatrix} = \begin{pmatrix} L_s & L_m \\ L_m & L_r \end{pmatrix}\begin{pmatrix} I_{dqs+}^{+} \\ I_{dqr+}^{+} \end{pmatrix} \quad (26)$$

While the dynamic equations of DFIG with negative sequence components can be described by the following equations sets [26]:

$$\begin{pmatrix} V_{ds-}^{-} \\ V_{qs-}^{-} \end{pmatrix} = R_s \begin{pmatrix} I_{ds-}^{-} \\ I_{qs-}^{-} \end{pmatrix} + \frac{d}{dt}\begin{pmatrix} \psi_{ds-}^{-} \\ \psi_{qs-}^{-} \end{pmatrix} + j\omega_s^{-}\begin{pmatrix} 0 & -1 \\ 1 & 0 \end{pmatrix}\begin{pmatrix} \psi_{ds-}^{-} \\ \psi_{qs-}^{-} \end{pmatrix}$$

$$\begin{pmatrix} V_{dr-}^{-} \\ V_{qr-}^{-} \end{pmatrix} = R_r \begin{pmatrix} I_{dr-}^{-} \\ I_{qr-}^{-} \end{pmatrix} + \frac{d}{dt}\begin{pmatrix} \psi_{dr-}^{-} \\ \psi_{qr-}^{-} \end{pmatrix} + j\omega_{sl}^{-}\begin{pmatrix} 0 & -1 \\ 1 & 0 \end{pmatrix}\begin{pmatrix} \psi_{dr-}^{-} \\ \psi_{qr-}^{-} \end{pmatrix}$$

$$\begin{pmatrix} \psi_{dqs-}^{-} \\ \psi_{dqr-}^{-} \end{pmatrix} = \begin{pmatrix} L_s & L_m \\ L_m & L_r \end{pmatrix}\begin{pmatrix} I_{dqs-}^{-} \\ I_{dqr-}^{-} \end{pmatrix} \quad (27)$$

where, $\omega_{sl}^{+} = \omega_s - \omega_r$ is the positive slip speed for positive reference frame, $\omega_s^{-} = -\omega_s$ is the synchronous speed of negative reference frame, and $\omega_{sl}^{-} = -\omega_{sl}^{+}$ is the negative slip speed for negative reference frame.

Similarly as depicted in conventional control scheme, Stator Flux Oriented Control (SFOC) will be implemented by aligning the positive direct axis of the synchronous reference frame along with the positive stator flux vector [27], this yields to:

$$\begin{cases} \psi_{ds+}^{+} = \psi_s^{+} \\ \psi_{qs+}^{+} = 0 \end{cases} \rightarrow \begin{cases} V_{ds+}^{+} = 0 \\ V_{qs+}^{+} = V_s^{+} \end{cases} \quad (28)$$

In the same manner for negative sequence control, SFOC will be adopted by aligning the negative direct axis of the synchronous reference frame along with the negative stator flux vector; this also yields to:

$$\begin{cases} \psi_{ds-}^{-} = \psi_s^{-} \\ \psi_{qs-}^{-} = 0 \end{cases} \rightarrow \begin{cases} V_{ds-}^{-} = 0 \\ V_{qs-}^{-} = V_s^{-} \end{cases} \quad (29)$$

By assuming that the stator resistance is neglected, the stator active and reactive powers can be calculated as in [24]:

$$\begin{cases} P_s = P_{so} + P_{ssine2}\,sin(2\omega_s t) + P_{scos2}\,cos(2\omega_s t) \\ Q_s = Q_{so} + Q_{ssine2}\,sin(2\omega_s t) + Q_{scos2}\,cos(2\omega_s t) \end{cases} \quad (30)$$

where, P_{so} & Q_{so} are the dc average values of stator active and reactive powers, while P_{ssine2}, P_{scos2}, Q_{ssine2}, and Q_{scos2} are the pulsating terms of DFIG's stator active & reactive powers at double grid frequency. It is noted that stator active and reactive power contain double grid frequency terms during DFIG unbalanced operation. These terms are described in the following matrixes [24]:

$$\begin{pmatrix} P_{so} \\ Q_{ssine2} \\ Q_{scos2} \end{pmatrix} = \frac{3L_m\,\omega_s}{2L_s}.\begin{pmatrix} -\psi_{qs+}^{+} & \psi_{ds+}^{+} & \psi_{qs-}^{-} & -\psi_{ds-}^{-} \\ -\psi_{qs-}^{-} & \psi_{ds-}^{-} & -\psi_{qs+}^{+} & \psi_{ds+}^{+} \\ -\psi_{ds-}^{-} & -\psi_{qs-}^{-} & \psi_{ds+}^{+} & -\psi_{qs+}^{+} \end{pmatrix} \begin{pmatrix} I_{dr+}^{+} \\ I_{qr+}^{+} \\ I_{dr-}^{-} \\ I_{qr-}^{-} \end{pmatrix} \quad (31)$$

$$\begin{pmatrix} Q_{so} \\ P_{ssine2} \\ P_{scos2} \end{pmatrix} = \frac{3\omega_s}{2L_s}.\begin{pmatrix} -\psi_{ds+}^{+} & -\psi_{qs+}^{+} & \psi_{ds-}^{-} & \psi_{qs-}^{-} \\ \psi_{ds-}^{-} & \psi_{qs-}^{-} & \psi_{ds+}^{+} & \psi_{qs+}^{+} \\ -\psi_{qs-}^{-} & \psi_{ds-}^{-} & \psi_{qs+}^{+} & -\psi_{ds+}^{+} \end{pmatrix} \left[\begin{pmatrix} \psi_{ds+}^{+} \\ \psi_{qs+}^{+} \\ \psi_{ds-}^{-} \\ \psi_{qs-}^{-} \end{pmatrix} - L_m.\begin{pmatrix} I_{dr+}^{+} \\ I_{qr+}^{+} \\ I_{dr-}^{-} \\ I_{qr-}^{-} \end{pmatrix}\right] \quad (32)$$

The electromagnetic torque also can be calculated as in [24]:

$$T_{em} = T_{emo} + T_{emsine2}\,sin(2\omega_s t) + T_{emcos2}\,cos(2\omega_s t) \quad (33)$$

where, T_{emo} is the DC average values of the electromagnetic torque, while $T_{emsine2}$, T_{emcos2} are the pulsating terms of electromagnetic torque at double grid frequency.

It is noted that the electromagnetic torque also contains double grid frequency terms during DFIG unbalance operation. These terms are described in the following matrix:

$$\begin{pmatrix} T_{emo} \\ T_{emsine2} \\ T_{emcos2} \end{pmatrix} = \frac{-3L_m}{2L_s} \cdot \begin{pmatrix} -\psi^{+}_{qs+} & \psi^{+}_{ds+} & \psi^{-}_{qs-} & -\psi^{-}_{ds-} \\ -\psi^{-}_{ds-} & -\psi^{-}_{qs-} & -\psi^{+}_{ds+} & \psi^{+}_{qs+} \\ \psi^{-}_{qs-} & -\psi^{-}_{ds-} & \psi^{+}_{qs+} & -\psi^{+}_{ds+} \end{pmatrix} \begin{pmatrix} I^{+}_{dr+} \\ I^{+}_{qr+} \\ I^{-}_{dr-} \\ I^{-}_{qr-} \end{pmatrix} \quad (34)$$

We can conclude that when DFIG is working under unbalanced conditions, double grid frequency terms (of 100Hz) will exist in both torque and stator power. These pulsating terms are usually proportional to the unbalance grid conditions status level. It is also obvious from the above expressions that in order to enhance DFIG operation during unbalanced conditions, the twice frequency terms in torque & power should be eliminated or reduced by controlling and regulating negative sequence components of DFIG rotor side voltages and currents as to tend to zero or lower values.

The control scheme strategy adopted in this paper employs a main controller and an auxiliary controller. The main controller is designed in the same manner as described in the conventional control scheme to control and operate the DFIG in the positive dq reference frame during balanced conditions. The auxiliary controller is implemented in the negative dq reference frame to control the negative sequence currents during unbalanced conditions. The Voltage Unbalance Detector (VUD) is used to detect the presence of unbalance voltage and to calculate the existing unbalance percentage. When this percentage exceeds a predefined threshold, the auxiliary controller immediately is switched on to handle this situation. The implemented control strategy is described in Fig. 6.

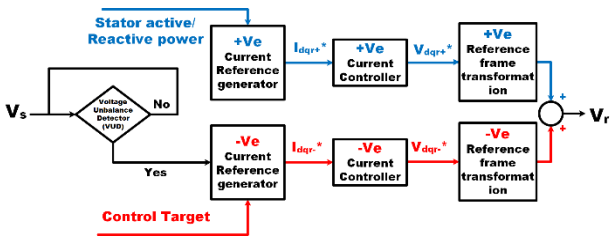

Figure 6. Structure of the applied dual control scheme

V. Simulation Results and Discussions

Wind turbine model is developed and implemented in Matlab/Simulink. The developed model is applicable for wide range of wind turbines. It is tested on G52/850 kW variable wind speed turbine, whose specification data is listed in Table II. Fig. 7 depicts the mechanical output power and the power coefficient at each wind speed. The simulated model results are evaluated and compared with its corresponding results in [19] to ensure its validity.

The model of DFIG-based WECS is developed and implemented in Matlab/Simulink. It is tested on real data of 850 kW DFIG machines, specification data for 850 kW DFIG machine is also tabulated in Table II [19], [29]. It is also validated in the same manner by evaluating and comparing its performance with its corresponding results in [17], [18].

TABLE II. Parameters of 850kW Wind Turbine & DFIG Machine [19], [29]

850kW wind turbine specifications		850kW DFIG machine data	
Rated Power	850kW	Voltage and Freq.	690V, 50Hz
Cut-in wind Speed	4m/s	Pole pairs	2
Nominal wind Speed	16m/s	Stator resistance	0.00332Ω
Cut-out wind Speed	25m/s	Rotor resistance	0.00278Ω
Blade radius	24m	Stator inductance	0.00649H
Turbine rotor speed	14.6-26.2rpm	Rotor inductance	0.00652H
Number of blades	3	Mutual inductance	0.00641H
Air density	1.225Kg/m^3	Inertia	30Kg.m^2

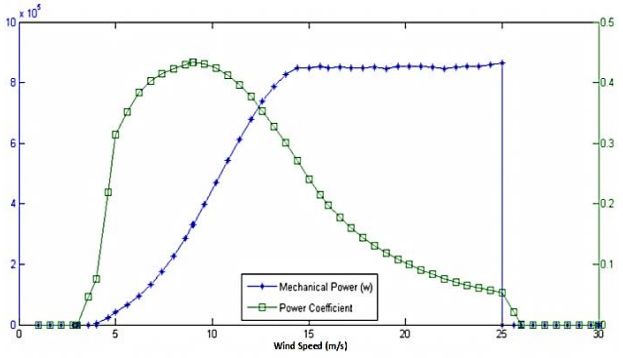

Figure 7. Mechanical power and power coefficient versus wind speed

Extensive simulation results are carried out using Matlab/Simulink for 850kW DFIG machine during balanced and unbalanced grid voltage conditions in order to verify the applied dual reference frame control scheme and to evaluate the behavior of DFIG within such different situations.

Finally Al-Zafarana wind farm (phase-5), which consists of 100 wind turbines with 850kW DFIG machine with each turbine, is implemented and simulated using Digsilent/PowerFactory software to study the behavior of this large system during balanced and unbalanced grid voltage conditions.

Some general assumptions have been taken into consideration; the grid disturbances are considered of short duration whose maximum value is a few hundred of milliseconds. The wind speed is assumed to be constant since the grid disturbance is of small time change and it is faster than wind speed variations. The impact of pitch angle regulation is ignored and the input mechanical governor torque to DFIG is considered constant.

A. 850kW DFIG Performance Results

Many simulation tests have been carried out to verify the DFIG performance at wind variations (high, medium, and low) and VAR regulation. MPPT technique is

applied on this case study model by providing lookup table that supplies the rotor side converter controller with reference generator rotational speed to keep and make the DFIG on this reference track to maximize and harvest maximum power from wind at lower wind speed values. Fig. 8 shows the response of rotational speed, electromagnetic torque, and active & reactive power within turbulence wind speed variations, and its capability to deliver rated active power to grid.

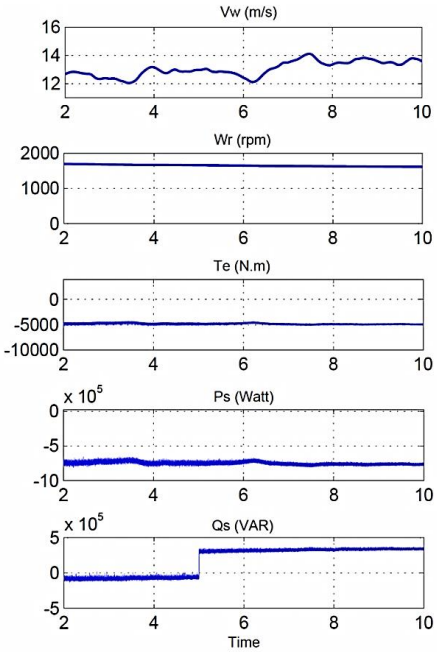

Figure 8. Response of 850kW DFIG during turbulence wind and VAR regulator

The results depicts DFIG behavior during turbulence wind speed values, and the control scheme capability to take control and deliver the output active & reactive power within rated production limits. Based on the achieved results, it reveals the machine capability to regulate reactive power according to grid network needs independently away from active power control. Hence it proves the reliability of vector oriented control scheme presented.

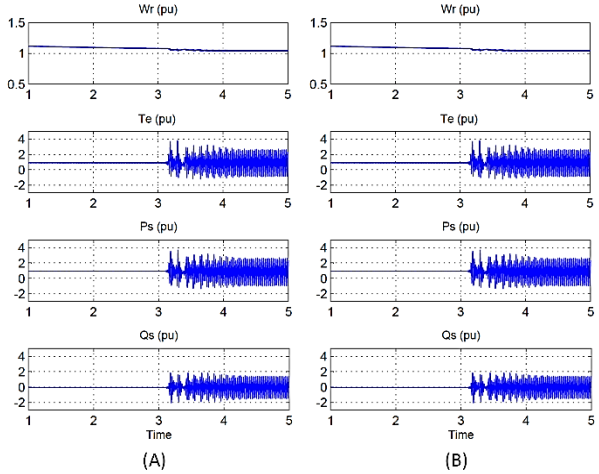

Figure 9. Response of 850kW DFIG without using the applied VUD dual control scheme at (A) 30% dip, and (B) 20% dip

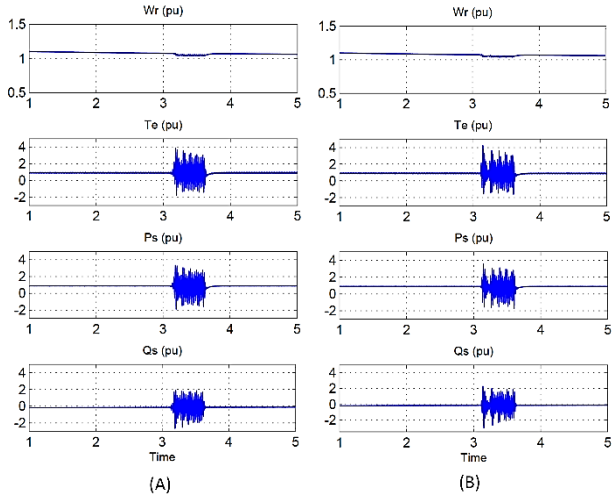

Figure 10. Response of 850kW DFIG with using the applied VUD dual control scheme at (A) 30% dip, and (B) 20% dip

Furthermore, the applied VUD dual reference control scheme is tested on DFIG model to investigate the DFIG response during unbalanced grid voltage conditions and to reduce the impacts of negative sequence effects on DFIG operation. Voltage dips of 30% and 20% have been applied on the implemented DFIG model at t=3.1sec with a clearance time of 400ms. Fig. 9 & Fig. 10 show the response of the 850kw DFIG machine without and with implementing the VUD dual control scheme respectively. The achieved results ensure that the DFIG applied control scheme could successfully control the machine after the clearance of the unbalance conditions and restore it again to normal operation status.

B. Case Study; Al-Zafarana Wind Farm Digsilent/Power-Factory Model Results

Al-Zafarana wind farm is established at Red Sea coast in south east of Cairo, Egypt. Phase-5 of Al-Zafarana is taken into account in this paper for analytical purposes. It is made up of 100 Gamesa G52/850kW variable speed wind turbines which employ DFIG, with total rated power of 85MW and connected to the Egyptian unified 220kV grid by two OHTL [30]. The simplified electrical layout is shown in Fig. 11. The wind turbines with attached DFIGs are distributed within seven feeders, and each wind turbine set is connected to 690V/22kV local step up transformer. The collected electrical power is gathered from downward feeders and connected to Zafarana substation, which belongs to the Egyptian Electricity Transmission Company. It contains three 75MVA, 22/220kV main step up transformers, that connect the entire wind farm to the 220kV network.

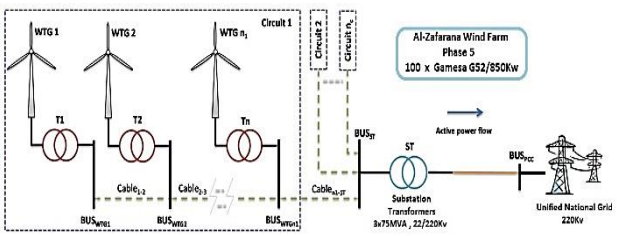

Figure 11. Simplified layout of Phase-5 of Al-Zafarana wind farm

A series of simulations has been carried out on this wind farm to evaluate its performance during balanced and unbalanced grid conditions. A load of 10MVA, which represents the auxiliary equipment loads of the wind farm, is attached to the network at 220kV (1 p.u) bus bar and is directly supplied by the wind farm.

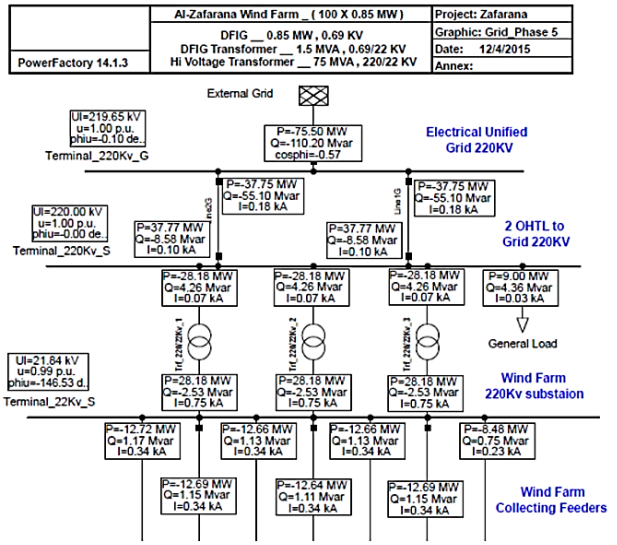

Figure 12. Load power flow of Al-Zafarana wind farm at balanced conditions

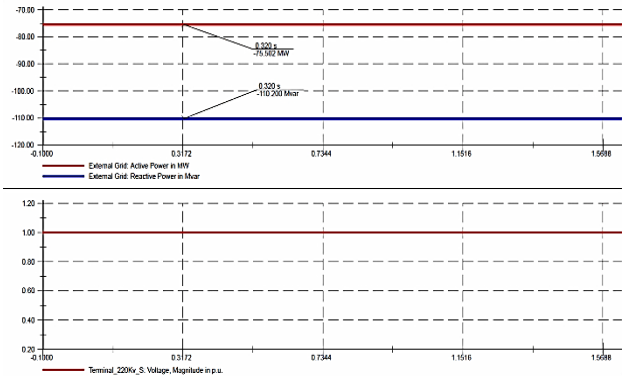

Figure 13. Grid readings at balanced conditions

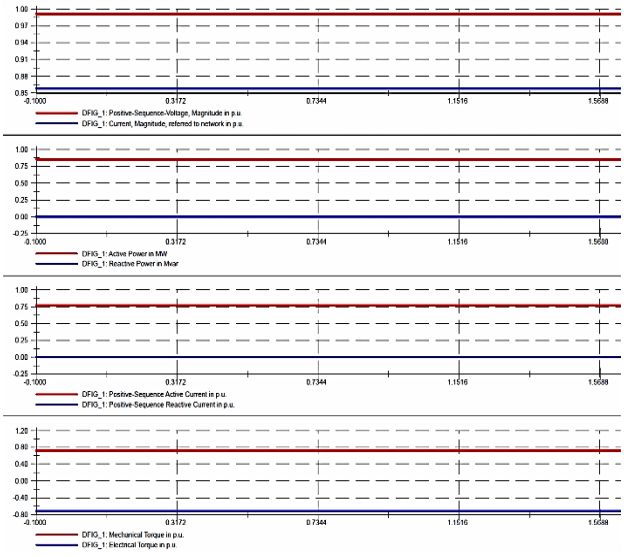

Figure 14. DFIG No. 1 performance at balanced conditions

At balanced grid voltage conditions, the load power flow of the entire wind farm is described in Fig. 12, showing all corresponding data for all equipments. While Figs. 13 & 14 depict the performance of the grid and one wind turbine within the farm as a sample (DFIG No. 1), which are in stable operation as noted at its rated nominal values.

Three Single Line to Ground (SLG) faults are assumed to be occurred on one OHTL that connects the farm to the 220kV grid (Line 1_G) at different time instants. The simulated faults are of different fault resistances; at t_1=0.31 sec with R_{fault}=5Ω, t_2=0.73 sec with R_{fault}=10Ω, and t_3=1.15 sec with R_{fault}=15Ω. The fault clearance time is considered 120 ms for all faults.

Figs. 15 & 16 depict the performance of the grid and one wind turbine within the farm (DFIG No. 1) as a sample. It is noted that the three SLG faults have caused voltage dip of 50%, 30%, and 20% at DFIG line terminal voltage respectively based on the fault resistance value for each fault case. The more voltage dip depth, the more pulsations of active, reactive, and electromagnetic torque occur on DFIG terminals.

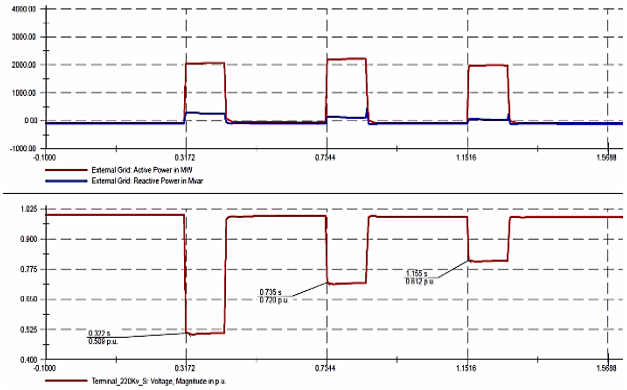

Figure 15. Grid readings at unbalanced conditions for the three faults

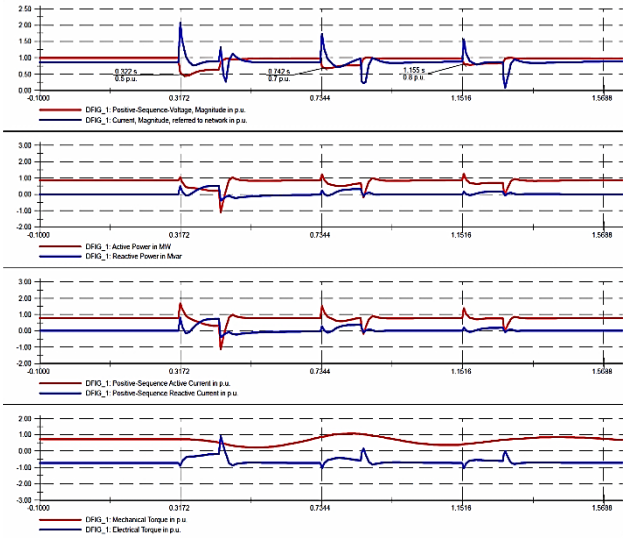

Figure 16. DFIG No. 1 performance at unbalanced conditions the three faults

At each fault case, the voltage at the DFIG machine terminal drops and affects directly decreasing the stator and rotor flux and therefore as a result, a reduction of

active power and electromagnetic torque occur. DFIG demagnetizes all energy stored at the fault instant into stator winding by reactive power peaks. The generator rotational speed will accelerate due to the electromagnetic torque decreasing and its associated torque drops with mechanical torque.

When the fault is cleared, the normal conditions of wind farm are successfully restored again for the three tested fault cases; the stator voltage, the active & reactive power, and the electromagnetic torque have been recovered to their initial values before fault occurrence.

VI. Conclusion

In this paper, a dynamic DFIG-based WECS is developed and implemented in Matlab/Simulink. The model is tested on real data of Gamesa G52/850kW DFIG machine which is used in Phase-5 of Al-Zafarana wind farm in Egypt.

Conventional control scheme for Rotor Side Converter (RSC) is developed in dq synchronous reference frame and applied on DFIG model to independently control stator active (or rotational speed) and stator reactive power by acting on quadrature and direct components of rotor current respectively. The conventional control scheme is capable to control DFIG machine within rated production limits during wind turbulence and reactive power regulations. However, it couldn't be able to control or handle the impacts of negative sequence components as in torque and power pulsations at unbalanced grid voltage conditions.

A dual reference frame control scheme is applied to improve the behavior of DFIG operation during unbalance conditions. It adopts two controllers; main controller that is designed in the same manner as in conventional control scheme to regulate positive sequence components during balanced conditions, and auxiliary controller to mitigate the negative sequence components effects on DFIG performance, by acting on negative sequence components in rotor currents. Voltage Unbalance Detector (VUD) is employed to detect the presence of unbalance grid voltage conditions. The auxiliary controller is only switched on when unbalance voltage exceeds risk limits and switched off again after the clearance of unbalance voltage conditions.

Simulation tests have been executed at different conditions to test the dynamic performance of DFIG-based WECS. The achieved results reveal the capability of the applied control scheme to control DFIG machine effectively during unbalance grid conditions by restoring the DFIG machine again with its normal status as it was before unbalanced grid conditions.

The 5th phase of Al-Zafarana wind farm (85MW) is also implemented using Digsilent/PowerFactory simulation tool. Simulations have been accomplished on it during balanced and unbalanced grid conditions to check the dynamic performance of wind farm interaction with power grid utility. Three different SLG faults conditions have been simulated to be occurred on one OHTL that connects the wind farm with the grid network. These faults conditions have exported voltage dips of 50%, 30%, and 20% values on DFIG terminal voltage. Results show that the more voltage dip depth, the more power and torque pulsations occur at the starting and ending time of fault case.

References

[1] T. Ackermann, *Wind Power in Power Systems*, John Wiley & Sons Ltd, 2005.

[2] B. Wu, Y. Lang, N. Zargari, and S. Kouro, *Power Conversion and Control of Wind Energy Systems*, John Wiley & Sons Ltd, 2011.

[3] G. Abad, J. Lopez, M. Rodriguez, L. Marroyo, and G. Iwanski, *Doubly Fed Induction Machine*, John Wiley & Sons Ltd, 2011.

[4] S. Muller, M. Deicke, and R. Doncker, "Doubly fed induction generator systems for wind turbines," *IEEE Transaction on Industry Application Magazine*, vol. 8, no. 3, pp. 26-33, May/June 2002.

[5] (March 2014). Wind farm grid connection code in addition to the Egyptian Transmission Grid Code (ETGC). [Online]. Available: www.egyptera.org

[6] I. Erlich, H. Wrede, and C. Feltes, "Dynamic behavior of DFIG-based wind turbines during grid faults," in *Proc. IEEE Conference on Power Conversion Conference*, Nagoya, April 2007, pp. 1195-1200.

[7] A. El-Sattar, N. Saad, and M. S. El-Dine, "Dynamic response of doubly fed induction generator variable speed wind turbine under fault," *Electric Power Systems Research*, no. 78, pp. 1240-1246, 2008.

[8] E. Muljadi, C. Butterfield, T. Batan, and D. Yildirim, "Understanding the unbalanced-voltage problem in wind turbine generation," in *Proc. IEEE Conference on Industry Application Magazine*, October 1999.

[9] I. Erlich and F. Shewarega, "Introduction of wind power generation into the first course in power systems," in *Proc. IEEE Conference on Power Engineering Society General Meeting*, Tampa, June 2007.

[10] R. Pena, J. Clare, and G. Asher, "Doubly fed induction generator using back-to-back PWM converters and its application to variable speed," *IEEE Transaction on Industry Application Magazine*, vol. 8, no. 3, pp. 26-33, May/June 2002.

[11] A Manyonge, R. Ochieng, F. Onyango, and J. Shichikha, "Mathematical modelling of wind turbine in a wind energy conversion system: Power coefficient analysis," *Applied Mathematical Sciences*, vol. 6, no. 91, pp. 4527-4536, 2012.

[12] I. Erlich and F. Shewarega., "Modeling of wind turbines equipped with doubly-fed induction machines for power system stability studies," in *Proc. IEEE Conference on Power Systems Conference & Exposition*, Atlanta, Nov. 2006, pp. 978-985.

[13] I. Erlich, J. Kretschmann, J. Fortmann, S. Mueller, and H. Wrede, "Modeling of wind turbines based on doubly-fed induction generators for power system stability studies," *IEEE Transactions on Power Systems*, vol. 22, no. 3, pp. 909-919, 2007.

[14] D. Fengfeng, H. Xueliang, Z. Ruihin, and Y. Zenghui, "Research on doubly-fed wind power generator modeling," in *Proc. IEEE Conference on Electricity Distribution*, Nanjing, Sept. 2010.

[15] R. M. V. Bapabla and D. S. Bankar, "Modeling of wind turbines based on DFIG for power system stability studies," in *Proc. National Conference on Challenges to Indian Power Scenario*, 24-25 Feb. 2011.

[16] A. V. Prabhugaonkar, *et al.*, "Modeling and analysis of DFIG wind turbine," *Journal of Engineering Research and Studies*, vol. 3, no. 2, pp. 72-76, April-June 2012.

[17] K. Kerrouche, A. Mezouar, L. Boumediene, and K. Belgacem, "Modeling and optimum power control based DFIG wind energy conversion system," *International Review of Electrical Engineering*, vol. 9, no. 1, pp. 174-185, Feb. 2014.

[18] T. Masaud and P. K. Sen, "Modeling and control of doubly fed induction generator for wind power," in *Proc. IEEE Conference on North American Power Symposium*, Boston, Sept. 2011.

[19] O. Badran, E. Abdulhadi, and R. Mamlook. Evaluation of parameters affecting wind turbine power generation. Ontario Sustainable Energy Association, (OSEA). [Online]. Available: http://www.ontario-sea.org/Storage/27/1883_Evaluation_of_parameters_affecting_wind_turbine_power_generation.pdf

[20] J. Lopez, P. Sanchis, X. Roboam, and L. Marroyo, "Dynamic behavior of the doubly fed induction generator during three-phase voltage dips," *IEEE Transactions on Energy Conversion*, vol. 22, no. 3, pp. 709-717, Sept. 2007.
[21] J. Lopez, E. Gubia, P. Sanchis, X. Roboam, and L. Marroyo, "Wind turbines based on doubly fed induction generator under asymmetrical voltage dips," *IEEE Transactions on Energy Conversion*, vol. 23, no. 1, pp. 321-330, Feb. 2008.
[22] A. Perdana, O. Carlson, and J. Persson, "Dynamic response of grid-connected wind turbines with doubly fed induction generator during disturbances," in *Proc. Nordic Workshop on Power and Industrial Electronics*, Trondheim, Feb. 2004.
[23] Y. Yasa, E. Isen, Y. Sozer, E. Mese, and H. Gurleyen, "Analysis of doubly fed induction generator wind turbine system during one phase-to-ground fault," in *Proc. IEEE Conference on Power Electronics and Applications*, Lille, Sept. 2013.
[24] L. Xu and Y. Wang, "Dynamic modeling and control of DFIG based wind turbines under unbalanced network conditions," *IEEE Transactions on Power Systems*, vol. 22, no. 1, pp. 314-323, Feb. 2007.
[25] L. Xu and Y. Wang, "Control of DFIG-based wind generation systems under unbalanced network supply," in *Proc. IEEE Conference on Electric Machines & Drives*, Antalya, May 2007, pp. 430-435.
[26] S. Hu and X. Zou, "An enhanced control scheme for unbalanced operation of doubly-fed induction generator," in *Proc. IEEE Conference on Power Electronics and Motion Control*, Harbin, June 2012, pp. 2134-2140.
[27] H. Xiao and F. Liu, "A control strategy of DFIG under unbalanced grid voltage," *Elektronika IR Elektronika*, vol. 19, no. 9, pp. 15-20, 2013.
[28] S. Yang, L. Zhan, C. Huang, and Z. Xie, "Unbalanced control system design for DFIG-based wind turbines," in *Proc. IEEE Conference on Power Engineering and Automation*, Wuhan, Sept. 2012.
[29] K. Taha, S. Tawfeic, and A. Hegazy, "Pitch control of a wind turbine rotor blade," *Minia Journal of Engineering and Technology*, vol. 32, no. 2, pp. 27-35, 2013.
[30] T. A. Kawady, "An interactive simulation of grid-connected DFIG units for protective relaying studies," in *Proc. IEEE Conference on Sustainable Alternative Energy*, Valencia, Sept. 2009.

Khaled Hamza El-Sayed was born in Cairo, Egypt, on October 28, 1985. He received his B.Sc. degree in Electrical Power and Machines Engineering from Cairo University, Egypt, in 2007. From 2007 to 2009, he was an Electrical design Engineer at Engineering Dept. of Petrokima Company, Cairo, Egypt. From 2009 to 2015, he has joined Cairo Electricity Production Company, where he worked as an Electrical Operation Engineer at Cairo West thermal Power Station. Since 2015 he is with Saudi Binladin Group (SBG), Makkah, KSA, presently and Electromechanical Coordinator Engineer for Holy Haram Special Package systems, such as PV modules, Fa ҫade Doors, and Sliding Domes.

Doaa Khalil Ibrahim (IEEE M'06, SM'13) was born in Egypt in December 1973. She received the M.Sc. and Ph.D. degrees in digital protection from Cairo University, Egypt, in 2001 and 2005, respectively. From 1996 to 2005, she was a Demonstrator and Research Assistant with Cairo University. In 2005, she became an Assistant Professor with Cairo University. In 2011, she became an Associate Professor with Cairo University. Since 2009, she has contributed to the Program of Continuous Improvement and Qualifying for Accreditation in Higher Education in Egypt. Her research interests include digital protection of power system as well as utilization and generation of electric power, distributed generation and renewable energy sources.

Essam EL-Din Abou EL-Zahab received the BSc. and MSc. degrees in electrical power and machines from Cairo University, Egypt, in 1970 and 1974, respectively. He received the PhD. degree in Electrical Power from Paul Sabatier, Toulouse France, in 1979. Currently he is a Professor in the Department of Electrical Power and Machines at Cairo University. His research areas include protection system, renewable energy, and power distribution. He is also the author or co-author of many referenced journal and conference papers.